

# Quantum Sampling Algorithms for Near-Term Devices

Dominik S. Wild,<sup>1</sup> Dries Sels,<sup>1</sup> Hannes Pichler,<sup>1,2</sup> Cristian Zanoci,<sup>3</sup> and Mikhail D. Lukin<sup>1</sup>

<sup>1</sup>*Department of Physics, Harvard University, Cambridge, Massachusetts 02138, USA*

<sup>2</sup>*Department of Physics, California Institute of Technology, Pasadena, California 91125, USA*

<sup>3</sup>*Department of Physics, Massachusetts Institute of Technology, Cambridge, Massachusetts 02139, USA*

(Dated: November 20, 2021)

Constructing and implementing useful quantum algorithms is one of the central challenges in quantum information science. Efficient sampling from a classical Gibbs distribution is an important computational problem with applications ranging from statistical physics over Monte Carlo and optimization algorithms to machine learning. Here, we introduce a family of quantum algorithms that provide unbiased samples by preparing a state that encodes the entire Gibbs distribution. We show that this approach leads to a speedup over a classical Markov chain for several examples including the Ising model and sampling from weighted, independent sets of two different graphs. We further propose a realistic implementation of sampling from independent sets based on Rydberg atom arrays. Our approach connects computational complexity with phase transitions, providing a physical interpretation of quantum speedup, and opens the door to exploring potentially useful sampling algorithms using near-term quantum devices.

Efficient algorithms that sample from Gibbs distributions are of broad practical importance in areas including statistical physics [1], optimization [2], and machine learning [3]. Quantum systems are naturally suited for encoding sampling problems: according to the Born rule, a projective measurement of a quantum state  $|\psi\rangle$  in an orthonormal basis  $\{|s\rangle\}$  yields a random sample drawn from the probability distribution  $p(s) = |\langle s|\psi\rangle|^2$ . This observation underpins recent work aiming to demonstrate quantum advantage over classical computers by sampling from a probability distribution defined in terms of a quantum gate sequence [4] or an optical network [5]. While these efforts have led to impressive experimental demonstrations [6, 7], thus far they have limited implications for practically relevant problems.

In this Article, we introduce a family of quantum algorithms for sampling from classical Gibbs distributions. We illustrate our approach with several specific examples including sampling from the Ising model and weighted independent sets. Since approximating the size of the maximum independent set on a random graph is NP hard [8], the latter case encompasses computationally hard problems, which are potentially relevant for applications such as computer vision [9], biochemistry [10], and social networks [11]. Before proceeding, we note that several quantum algorithms for sampling problems have been developed previously [12–22]. In contrast to many of these pioneering proposals, our approach does not require a large-scale, universal quantum computer and may be realized on relatively near-term quantum devices.

The key ideas for our approach are summarized in Fig. 1. We consider a system of  $n$  classical bits, labeling a complete bit string by  $s$ . We focus on spin models, where  $s = s_1 s_2 \dots s_n$  with each spin being either up ( $s_i = +1$ ) or down ( $s_i = -1$ ). The desired Gibbs distribution  $p_\beta(s) = e^{-\beta H_c(s)}/\mathcal{Z}$  is defined in terms of the energies  $H_c(s)$  and the inverse temperature  $\beta$  with

$\mathcal{Z} = \sum_s e^{-\beta H_c(s)}$  denoting the partition function. Sampling from a classical Gibbs distribution can be reduced to preparing the quantum state

$$|\psi(\beta)\rangle = \frac{1}{\sqrt{\mathcal{Z}}} \sum_s e^{-\beta H_c(s)/2} |s\rangle, \quad (1)$$

referred to as the Gibbs state, followed by a projective measurement in the  $\{|s\rangle\}$  basis. To prepare this state, we start from a classical Markov chain Monte

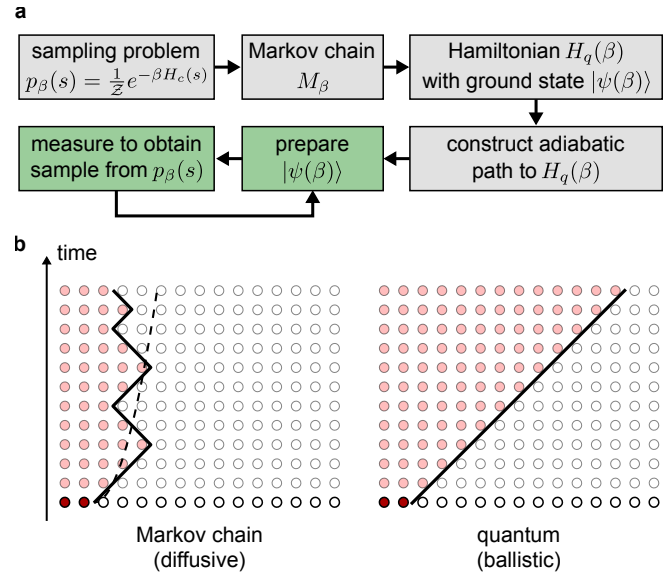


**Fig. 1. Quantum algorithms to sample from classical Gibbs distributions.** **a**, Key steps in the construction of the proposed quantum algorithms. The green boxes constitute the sampling procedure, which is carried out on a quantum computer. **b**, In two examples discussed below, the speedup of our algorithm can be understood to be due to ballistic propagation of domain walls in the quantum system as opposed to the diffusive random walk in the Markov chain.

Carlo algorithm for sampling from the Gibbs distribution. Any such Markov chain can be mapped onto a so-called parent Hamiltonian  $H_q(\beta)$  with the unique ground state  $|\psi(\beta)\rangle$  [23]. Next, we identify a sufficiently simple Hamiltonian  $H_0$  whose ground state can be readily prepared and which can be adiabatically deformed into  $H_q(\beta)$ , thereby producing the Gibbs state. In contrast to prior work [18], we do not restrict the adiabatic evolution to the one-parameter family of Hamiltonians defined by  $H_q(\beta)$  for arbitrary  $\beta$ . Instead, as shown below, more general paths allow one to outperform adiabatic evolution along the one-parameter family and give rise to an asymptotic speedup over the classical Markov chain.

In two of the examples presented below, the origin of the speedup can be understood as resulting from ballistic propagation of domain walls enabled by quantum coherent motion in contrast to the diffusion caused by classical thermal fluctuations. Since the width of the region explored by diffusion is proportional to the square root of time (dashed curve in Fig. 1b), we generically expect a quadratic speedup. Additional speedup is possible if diffusion in the Markov chain is suppressed, e.g. by a thermal barrier. An alternative speedup mechanism associated with quantum tunneling is uncovered in the independent set problem on star graphs.

## PARENT HAMILTONIANS

Our construction of the parent Hamiltonian follows the prescription in reference [23] (see references [24–26] for related earlier work). We first define a Markov chain that samples from the desired Gibbs distribution  $p_\beta(s)$ . The Markov chain is specified by a generator matrix  $M_\beta$ , where the probability distribution  $q_t(s)$  at time  $t$  evolves according to  $q_{t+1}(s) = \sum_{s'} q_t(s') M_\beta(s', s)$ . By construction,  $p_\beta(s)$  is a stationary distribution of the Markov chain and therefore constitutes a left eigenvector of  $M_\beta$  with eigenvalue unity. We assume in addition that the Markov chain satisfies detailed balance, which can be expressed as  $e^{-\beta H_c(s')} M_\beta(s', s) = e^{-\beta H_c(s)} M_\beta(s, s')$ . This property implies that

$$H_q(\beta) = n \left( \mathbb{I} - e^{-\beta H_c/2} M_\beta e^{\beta H_c/2} \right) \quad (2)$$

is a real, symmetric matrix. It can be viewed as a quantum Hamiltonian with the Gibbs state  $|\psi(\beta)\rangle$  being its zero-energy eigenstate. The Gibbs state is a ground state because the spectrum of  $H_q(\beta)$  is bounded from below by 0. For every eigenvalue  $n(1 - \lambda)$  of  $H_q(\beta)$ , there exists an eigenvalue  $\lambda$  of  $M_\beta$ , where  $\lambda \leq 1$  because  $M_\beta$  is a stochastic matrix. If the Markov chain is fully mixing and aperiodic, the Perron–Frobenius theorem [27] guarantees that  $|\psi(\beta)\rangle$  is the unique ground state of  $H_q(\beta)$ . The factor of  $n$  in equation (2) ensures that the spectrum of the parent Hamiltonian is extensive. To account for

the natural parallelization in adiabatic evolution, we divide the mixing time of the Markov chain by  $n$  for a fair comparison, denoting the result by  $t_m$ . The correspondence between the spectra of  $M_\beta$  and  $H_q(\beta)$  establishes the bound  $t_m \geq 1/\Delta(\beta)$ , where  $\Delta(\beta)$  is the gap between the ground state and first excited state of the parent Hamiltonian [28].

## SAMPLING FROM THE 1D ISING MODEL

We now illustrate this procedure by considering a ferromagnetic Ising model composed of  $n$  spins in one dimension. The classical Hamiltonian is given by  $H_c = -\sum_{i=1}^n \sigma_i^z \sigma_{i+1}^z$  with periodic boundary conditions, letting  $\sigma_{n+1}^z = \sigma_1^z$  and  $\sigma_0^z = \sigma_n^z$ . We choose Glauber dynamics as the Markov chain, in which at each time step, a spin is selected at random and its value is drawn from a thermal distribution with all other spins fixed [29]. Up to a constant, the corresponding parent Hamiltonian takes the form

$$H_q(\beta) = - \sum_{i=1}^n [h(\beta) \sigma_i^x + J_1(\beta) \sigma_i^z \sigma_{i+1}^z - J_2(\beta) \sigma_{i-1}^z \sigma_i^x \sigma_{i+1}^z], \quad (3)$$

where  $4h(\beta) = 1 + 1/\cosh(2\beta)$ ,  $2J_1(\beta) = \tanh(2\beta)$ , and  $4J_2(\beta) = 1 - 1/\cosh(2\beta)$  (see supplementary information (SI) for details and references [30, 31] for early derivations of this result). At infinite temperature ( $\beta = 0$ ), we have  $J_1 = J_2 = 0$  and  $h = 1/2$ . The ground state is a paramagnet aligned along the  $x$ -direction, which corresponds to an equal superposition of all classical spin configurations, consistent with the Gibbs distribution at infinite temperature. When the temperature is lowered, the parameters move along a segment of a parabola in the two-dimensional parameter space  $(J_1/h, J_2/h)$  shown by the red curve (ii) in Fig. 2a. We highlight that any point along the segment can be viewed as a generalized Rokhsar–Kivelson point [25, 32], where the Hamiltonian is by construction stoquastic and frustration free [26, 33].

The quantum phase diagram of the parent Hamiltonian for arbitrary values of  $h$ ,  $J_1$ , and  $J_2$  is obtained by performing a Jordan–Wigner transformation that maps equation (3) onto a free-fermion model [34, 35] (see SI). The distinct quantum phases are displayed in Fig. 2a. The model reduces to the transverse field Ising model on the  $J_2/h = 0$  axis, in which a phase transition from a paramagnet to a ferromagnet occurs at  $J_1/h = 1$ . Along the  $J_1/h = 0$  axis, the ground state undergoes a symmetry-protected topological phase transition at  $J_2/h = \pm 1$  from the paramagnet to a cluster-state-like phase [36]. We note that the tricritical point at  $(J_1/h, J_2/h) = (2, 1)$  describes the parent Hamiltonian corresponding to zero temperature ( $\beta \rightarrow \infty$ ).

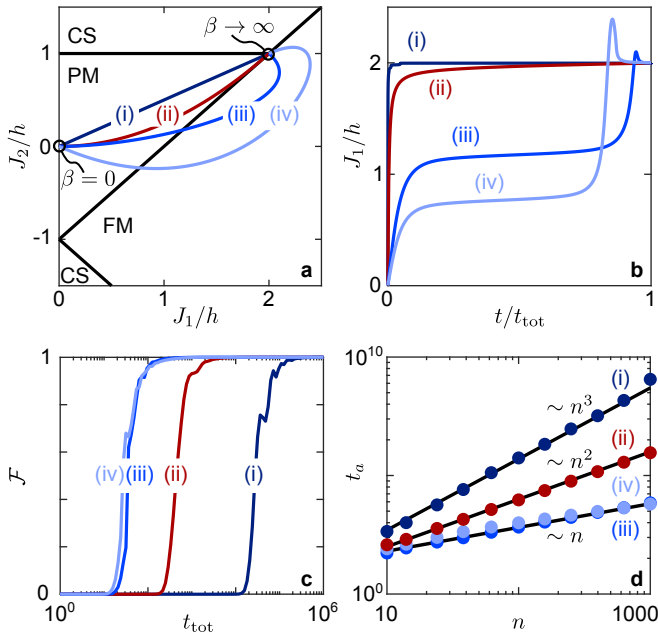


**Fig. 2. Sampling from the 1D Ising model.** **a**, Phase diagram of the parent Hamiltonian corresponding to the Ising chain. The black lines indicate the boundaries between paramagnetic (PM), ferromagnetic (FM), and cluster-state-like (CS) phases. The curves labeled (i)–(iv) show four different choices of adiabatic paths with (ii) representing the one-parameter family  $H_q(\beta)$ . **b**, The time dependence of  $J_1/h$  for a chain of  $n = 100$  spins according to equation (5) of the Methods section. **c**, Fidelity as a function of the sweep time along these trajectories. **d**, The time  $t_a$  required to reach a fidelity exceeding  $1 - 10^{-3}$  as a function of the number of spins  $n$ . The black lines are guides to the eye showing the expected linear, quadratic, and cubic dependencies of  $t_a$  on  $n$ .

To prepare the Gibbs state  $|\psi(\beta)\rangle$ , one may start from the ground state of  $H_q(0)$  before smoothly varying the parameters  $(h, J_1, J_2)$  to bring the Hamiltonian into its final form at the desired inverse temperature  $\beta$ . States with finite  $\beta$  can be connected to the infinite temperature state by a path that lies fully in the paramagnetic phase. Both adiabatic state preparation and the Markov chain are efficient in this case. Indeed, it has been shown previously that there exists a general quantum algorithm with run time  $\sim \log n$  for gapped parent Hamiltonians [22], which is identical to the Markov mixing time  $t_m$  for the Ising chain [37].

Sampling at zero temperature is more challenging with the mixing time of the Markov chain bounded by  $t_m \gtrsim n^2$  (see SI). For the quantum algorithm, we consider the four different paths in Fig. 2a. To evaluate the dynamics quantitatively, we choose the rate of change with the aim of satisfying the adiabatic condition at every point along the path (see Fig. 2b and Methods) and numerically integrate the Schrödinger equation with the initial state  $|\psi(0)\rangle$  to obtain  $|\phi(t_{\text{tot}})\rangle$  after total evolution time  $t_{\text{tot}}$  (without loss of generality we set  $\hbar = 1$ ). Figure 2c

shows the resulting fidelity  $\mathcal{F} = |\langle\phi(t_{\text{tot}})|\psi(\infty)\rangle|^2$  for a chain of  $n = 100$  spins. The total variation distance  $d = \|p - q\|$  between the desired Gibbs distribution and the prepared distribution  $q(s) = |\langle s|\phi(t_{\text{tot}})\rangle|^2$  is bounded by  $d \leq \sqrt{1 - \mathcal{F}}$  [38]. To determine the dependence on the number of spins, we extract the time  $t_a$  at which the fidelity exceeds  $1 - 10^{-3}$ , Fig. 2d. We find three different scalings of the time  $t_a$ : along path (i), it roughly scales as  $t_a \sim n^3$ , along (ii) as  $t_a \sim n^2$ , while (iii) and (iv) exhibit a scaling close to  $t_a \sim n$ .

These scalings follow from the nature of the phase transitions. The dynamical critical exponent at the tricritical point is  $z = 2$ , meaning that the gap closes with system size as  $\Delta \sim 1/n^2$ , which is consistent with the time required along path (ii). As shown in the SI, the dynamical critical exponent at all phase transitions away from the tricritical point is  $z = 1$  and the gap closes as  $\Delta \sim 1/n$ . Therefore, the paramagnetic to ferromagnetic phase transition can be crossed adiabatically in a time proportional to  $n$ , only limited by ballistic propagation of domain walls as opposed to diffusive propagation in the Markov chain. There is no quadratic slowdown as paths (iii) and (iv) approach the tricritical point, which we attribute to the large overlap of the final state with ground states in the ferromagnetic phase. Path (i) performs worse than path (ii) because the gap between the paramagnetic and cluster-state-like phases vanishes exactly for certain parameters even in a finite-sized system (see SI). To further support the statement that the speedup is of quantum mechanical origin, we note that the half-chain entanglement entropy of the ground state diverges logarithmically with the number of spins when paths (iii) and (iv) cross from the paramagnetic into the ferromagnetic phase. Hence, it is impossible to find a representation for the ground state at the phase transition in the form of equation (1) with a local, classical Hamiltonian  $H_c$  because any such representation would be a matrix product state with constant bond dimension and bounded entanglement entropy [23].

While this example illustrates a mechanism for quantum speedup, sampling from large systems is hard only at zero temperature [39]. Since sampling at zero temperature is equivalent to optimization, there may exist more suitable algorithms to solve the problem. In addition, the parent Hamiltonian, equation (3), does not have a simple physical realization. We address these limitations by considering the weighted independent set problem.

## WEIGHTED INDEPENDENT SETS

An independent set of a graph is any subset of vertices in which no two vertices share an edge, see Fig. 3a. We say vertex  $i$  is occupied if it is in the independent set and assign the occupation number  $n_i = 1$ . All other vertices are unoccupied with  $n_i = 0$ . In the weighted indepen-

dent set problem, each vertex is further assigned a weight  $w_i$  and we seek to minimize the energy  $H_c = -\sum_i w_i n_i$  subject to the independent set constraint. The corresponding Gibbs distribution has been studied extensively in probability theory and computer science [40] as well as in statistical physics [41, 42].

To construct a quantum algorithm, each vertex is associated with a spin variable  $\sigma_i^z = 2n_i - 1$ . Single spin flips with the Metropolis–Hastings update rule [43] yield the parent Hamiltonian

$$H_q(\beta) = \sum_i P_i [V_{e,i}(\beta)n_i + V_{g,i}(\beta)(1 - n_i) - \Omega_i(\beta)\sigma_i^x], \quad (4)$$

where we only consider the subspace spanned by the independent sets (see SI). In equation (4),  $P_i = \prod_{j \in \mathcal{N}_i} (1 - n_j)$  projects onto states in which the nearest neighbors  $\mathcal{N}_i$  of vertex  $i$  are all unoccupied. The remaining parameters are given by  $V_{e,i}(\beta) = e^{-\beta w_i}$ ,  $V_{g,i}(\beta) = 1$ , and  $\Omega_i(\beta) = e^{-\beta w_i/2}$ .

The projectors  $P_i$  involve up to  $d$ -body terms, where  $d$  is the degree of the graph. Nevertheless, they can be implemented e.g. using programmable atom arrays with minimal experimental overhead for certain classes of graphs. In the case of so-called unit disk graphs, Fig. 3a, these operators are naturally realizable using highly excited Rydberg states of neutral atoms (see Fig. 3b and Methods). As a simple example of a unit disk graph, we consider a chain of length  $n$  and choose equal weights  $w_i = 1$ . The resulting parent Hamiltonian has been studied both theoretically [44, 45] and experimentally using Rydberg atoms [46]. Its quantum phases can be characterized by the staggered magnetization  $M_k = (1/n) \sum_{j=1}^n e^{2\pi i j/k} \sigma_j^z$ . Figure 3c shows the ground state expectation value of  $|M_2| + |M_3|$  for  $n = 30$ , clearly indicating the presence of three distinct phases. For large  $\Omega/V_g$  or large, positive  $V_e/V_g$ , assuming  $V_g > 0$  throughout, the ground state respects the full translational symmetry of the Hamiltonian and  $|M_k|$  vanishes for all integers  $k > 1$ . When  $V_e/V_g$  is sufficiently small, the ground state is  $\mathbb{Z}_2$  ordered with every other site occupied and  $|M_2| \neq 0$ . Owing to next-to-nearest neighbor repulsive terms in the Hamiltonian, there further exists a  $\mathbb{Z}_3$  ordered phase, in which  $|M_3| \neq 0$  and the ground state is invariant only under translations by three lattice sites or multiples thereof.

The one-parameter family  $H_q(\beta)$  is indicated by the red curve (i) in Fig. 3c. We note that  $|\psi(0)\rangle$  is not a product state. However, the Hamiltonian  $H_q(0)$  can be adiabatically connected to  $\Omega/V_g = 0$  and  $V_e/V_g > 3$ , where the ground state is a product state of all sites unoccupied. Since such a path may lie fully in the disordered phase, adiabatic state preparation of the zero temperature Gibbs state is efficient. Similarly, the Markov chain at infinite temperature is efficient as the parent Hamiltonian is gapped. More generally, we show numerically

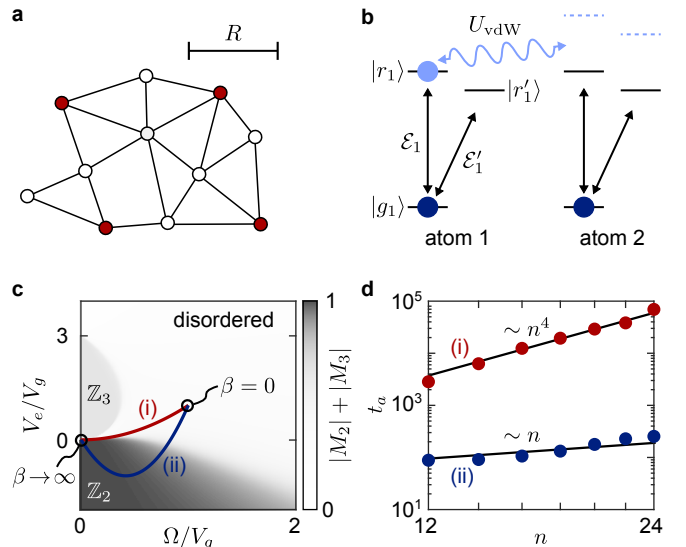


**Fig. 3. Sampling from independent sets of unit disk graphs.** **a**, Example of an independent set (red vertices) on a unit disk graph. Two vertices are connected if and only if they are separated by a distance less than  $R$ . **b**, Physical realization of the parent Hamiltonian, equation (4), using Rydberg blockade as discussed in the Methods section. The Hamiltonian parameters are determined by the drive amplitudes  $\mathcal{E}_i$  and  $\mathcal{E}'_i$  as well as their detuning from resonance. **c**, Parameter space and order parameter of the parent Hamiltonian for a chain of length  $n = 30$ . The order parameter  $|M_2| + |M_3|$  distinguishes the disordered phase from the  $\mathbb{Z}_2$  and  $\mathbb{Z}_3$  ordered phases. The red curve (i) indicates the one-parameter family  $H_q(\beta)$ , while the blue curve (ii) is an alternative adiabatic path crossing into the  $\mathbb{Z}_2$  phase. **d**, Adiabatic state preparation time  $t_a$  along the two paths in (c). Path (i) terminates at  $\beta_c = 2 \log n$  while (ii) continues to  $\beta \rightarrow \infty$ . The sweep rate was chosen according to equation (5) and the threshold fidelity was set to  $\mathcal{F} = 1 - 10^{-3}$ . The black lines are guides to the eye showing the scalings  $t_a \sim n$  and  $t_a \sim n^4$ .

in the SI that the gap is proportional to  $e^{-2\beta}$  at high temperature and  $e^{-\beta}/n^2$  at low temperature. In contrast to the Ising chain, the gap vanishes as  $\beta \rightarrow \infty$  even for finite sized systems. The physical reason is that defects in the  $\mathbb{Z}_2$  ordering must overcome an energy barrier to propagate. Since the Markov chain is not ergodic at zero temperature, it is only possible to sample approximately from the ground state by running the Markov chain at a low but nonzero temperature  $\beta \gtrsim \beta_c$ , where  $\beta_c = 2 \log n$  corresponds to the temperature at which the correlation length is comparable to the system size. The gap of the parent Hamiltonian bounds the mixing time by  $t_m \gtrsim e^{2\beta_c} \sim n^4$ . As shown in Fig. 3d, the adiabatic state preparation time along the one-parameter family  $H_q(\beta)$  appears to follow the same scaling.

A quantum speedup is obtained by choosing a different path. For example, an approximately linear scaling  $t_a \sim n$ , is observed along path (ii) in Fig. 3c. In analogy to the Ising chain, we attribute the linear scaling to the

dynamical critical exponent  $z = 1$  at the phase transition between the disordered and the  $\mathbb{Z}_2$  ordered phases. Note that for the independent set problem, the quantum speedup is quartic owing to the more slowly mixing Markov chain. We remark that it is possible to improve the performance of the Markov chain by adding simultaneous spin flips on neighboring sites, though the quantum algorithm still retains at least a quadratic speedup in this case similar to the Ising model (see Methods).

## SAMPLING FROM HARD GRAPHS

We next consider a graph for which it is hard to sample from independent sets even at nonzero temperature. The graph takes the shape of a star with  $b$  branches and two vertices per branch (see Fig. 2a). The weight of the vertex at the center is  $b$ , while all other weights are set to 1. The classical model exhibits a phase transition at  $\beta_c = \log \varphi \approx 0.48$ , where  $\varphi$  is the golden ratio (see Methods). Above the phase transition temperature, the free energy is dominated by the entropic contribution from the  $3^b$  states with the center unoccupied. Below the transition temperature, it is more favorable to decrease the potential energy by occupying the center at the cost of reducing the entropy as the independent set constraint limits the number of available states to  $2^b$  (see Fig. 4b).

The Markov chain on this graph has severe kinetic constraints since changing the central vertex from unoccupied to occupied requires all neighboring vertices to be unoccupied. Assuming that each individual branch is in thermal equilibrium, the probability of accepting such a move is given by  $p_{0 \rightarrow 1} = [(1 + e^\beta)/(1 + 2e^\beta)]^b$ . Similarly, the reverse process is energetically suppressed with an acceptance probability  $p_{1 \rightarrow 0} = e^{-b\beta}$ . The central vertex can thus become trapped in the thermodynamically unfavorable configuration, resulting in a mixing time that grows exponentially with  $b$  at any finite temperature. When starting from a random configuration, the Markov chain will nevertheless sample efficiently at high temperature because the probability of the central vertex being initially occupied is exponentially small. By the same argument, the Markov chain almost certainly starts in the wrong configuration in the low temperature phase and convergence to the Gibbs distribution requires a time  $t_m \gtrsim 1/p_{0 \rightarrow 1}$ .

The corresponding quantum dynamics are captured by a two-state model formed by  $|\psi_0(\beta)\rangle$  and  $|\psi_1(\beta)\rangle$ , which are Gibbs states with the central vertex fixed to be respectively unoccupied or occupied (see Fig. 4a and Methods). The tunneling rate between these states, i.e. the matrix element  $\langle \psi_0 | H_q | \psi_1 \rangle$ , is given by  $J = \Omega_{\text{cen}} \sqrt{p_{0 \rightarrow 1}}$ , where  $\Omega_{\text{cen}}$  denotes the coefficient  $\Omega_i$  in equation (4) associated with the central vertex. The time required to adiabatically cross the phase transition is bounded by  $t_a \gtrsim 1/J$  with  $J$  evaluated at the phase transition. Along

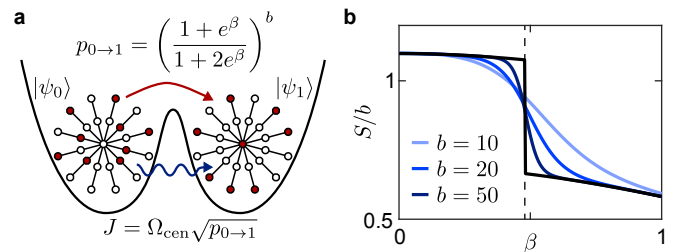


**Fig. 4. Hard sampling at nonzero temperature.** **a**, Sampling from a star graph with two vertices per branch is kinetically constrained because occupying the central vertex requires all adjacent vertices to be unoccupied. The mixing of the Markov chain is limited at low temperature by the probability  $p_{0 \rightarrow 1}$  of changing the central vertex from unoccupied to occupied. The quantum algorithm achieves a quadratic speedup over the Markov chain by tunneling between such configurations. **b**, Entropy per branch  $S/b$  of the Gibbs distribution corresponding to the weighted independent set problem on this star graph. The system exhibits a discontinuous phase transition at  $\beta_c \approx 0.48$  (dashed, vertical line). The central vertex is occupied with high probability when  $\beta > \beta_c$  and unoccupied otherwise. The blue curves were obtained for finite-sized systems, while the black curve indicates the thermodynamic limit (see Methods).

the one-parameter family  $H_q(\beta)$ , we have  $\Omega_{\text{cen}} = \sqrt{p_{1 \rightarrow 0}}$ . In addition, at the phase transition,  $p_{0 \rightarrow 1} = p_{1 \rightarrow 0}$  such that  $t_a \gtrsim 1/p_{0 \rightarrow 1}$ , yielding the same time complexity as the Markov chain that samples at the phase transition. However, the square-root dependence of the tunneling rate on  $p_{0 \rightarrow 1}$  immediately suggests that a quadratic speedup may be attainable by crossing the phase transition with  $\Omega_{\text{cen}} = 1$ . An example of such a path is provided in the SI along with a demonstration of the quadratic speedup by numerically evaluating the adiabatic state preparation time.

## OUTLOOK

Our approach to quantum sampling algorithms unveils a connection between computational complexity and phase transitions and provides physical insight into the origin of quantum speedup. The quantum Hamiltonians appearing in the construction are guaranteed to be local given that the Gibbs distribution belongs to a local, classical Hamiltonian and that the Markov chain updates are local. Consequently, time evolution under these quantum Hamiltonians can be implemented using Hamiltonian simulation [47]. Moreover, a hardware efficient implementation in near-term devices may be possible for certain cases such as the independent set problem. While the proposed realization utilizing Rydberg blockade is restricted to unit disk graphs, a wider class of graphs may be accessible using anisotropic interactions [48] and individual addressing with multiple atomic sublevels [49].

Our approach can be extended along several directions. These include quantum algorithms corresponding to Markov chains with cluster updates, which are often effective in practice. To address practically relevant sampling problems, our method should be expanded to disordered systems in two or more dimensions, where it may be challenging to directly identify an efficient adiabatic path. Extensions to hybrid algorithms that combine quantum evolution with classical optimization may offer a solution to this problem. For instance, the energy of the parent Hamiltonian  $H_q(\beta)$  could be minimized using variational quantum algorithms, similar to previous proposals that directly minimize the free energy [50], without requiring complex measurements of the entanglement entropy. Apart from testing such algorithms, their realization on near-term quantum devices can open the door to exploration of novel applications in areas ranging from physical science to machine learning.

---

[1] Landau, L. D. & Lifshitz, E. M. *Statistical Physics* (Butterworth-Heinemann, Oxford, 1980), 3rd edn.

[2] Kirkpatrick, S., Gelatt, C. D. & Vecchi, M. P. Optimization by Simulated Annealing. *Science* **220**, 671–680 (1983).

[3] Bishop, C. M. *Pattern Recognition and Machine Learning* (Springer, New York, NY, 2006).

[4] Bouland, A., Fefferman, B., Nirkhe, C. & Vazirani, U. On the complexity and verification of quantum random circuit sampling. *Nat. Phys.* **15**, 159–163 (2018).

[5] Aaronson, S. & Arkhipov, A. The computational complexity of linear optics. In *STOC '11: Proceedings of the Forty-Third Annual ACM Symposium on Theory of Computing*, 333–342 (ACM Press, New York, NY, 2011).

[6] Arute, F. *et al.* Quantum supremacy using a programmable superconducting processor. *Nature* **574**, 505–510 (2019).

[7] Wang, H. *et al.* Boson Sampling with 20 Input Photons and a 60-Mode Interferometer in a  $10^{14}$ -Dimensional Hilbert Space. *Phys. Rev. Lett.* **123**, 250503 (2019).

[8] Garey, M. R. & Johnson, D. S. *Computers and Intractability: A Guide to the Theory of NP-Completeness* (W. H. Freeman & Co., New York, NY, 1979).

[9] Bomze, I. M., Budinich, M., Pardalos, P. M. & Pelillo, M. The Maximum Clique Problem. In *Handbook of Combinatorial Optimization*, 1–74 (Springer, Boston, MA, 1999).

[10] Butenko, S. & Wilhelm, W. Clique-detection models in computational biochemistry and genomics. *Eur. J. Oper. Res.* **173**, 1–17 (2006).

[11] Fortunato, S. Community detection in graphs. *Phys. Rep.* **486**, 75–174 (2010).

[12] Lidar, D. A. & Biham, O. Simulating Ising spin glasses on a quantum computer. *Phys. Rev. E* **56**, 3661–3681 (1997).

[13] Terhal, B. M. & DiVincenzo, D. P. Problem of equilibration and the computation of correlation functions on a quantum computer. *Phys. Rev. A* **61**, 022301 (2000).

[14] Bilgin, E. & Boixo, S. Preparing Thermal States of Quantum Systems by Dimension Reduction. *Phys. Rev. Lett.* **105**, 170405 (2010).

[15] Temme, K., Osborne, T. J., Vollbrecht, K. G., Poulin, D. & Verstraete, F. Quantum Metropolis sampling. *Nature* **471**, 87–90 (2011).

[16] Yung, M.-H. & Aspuru-Guzik, A. A quantum–quantum Metropolis algorithm. *Proc. Natl. Acad. Sci.* **109**, 754–759 (2012).

[17] Riera, A., Gogolin, C. & Eisert, J. Thermalization in Nature and on a Quantum Computer. *Phys. Rev. Lett.* **108**, 080402 (2012).

[18] Somma, R. D., Batista, C. D. & Ortiz, G. Quantum Approach to Classical Statistical Mechanics. *Phys. Rev. Lett.* **99**, 030603 (2007).

[19] Somma, R. D., Boixo, S., Barnum, H. & Knill, E. Quantum Simulations of Classical Annealing Processes. *Phys. Rev. Lett.* **101**, 130504 (2008).

[20] Wocjan, P. & Abeyesinghe, A. Speedup via quantum sampling. *Phys. Rev. A* **78**, 042336 (2008).

[21] Yung, M.-H., Nagaj, D., Whitfield, J. D. & Aspuru-Guzik, A. Simulation of classical thermal states on a quantum computer: A transfer-matrix approach. *Phys. Rev. A* **82**, 060302 (2010).

[22] Ge, Y., Molnár, A. & Cirac, J. I. Rapid Adiabatic Preparation of Injective Projected Entangled Pair States and Gibbs States. *Phys. Rev. Lett.* **116**, 080503 (2016).

[23] Verstraete, F., Wolf, M. M., Perez-Garcia, D. & Cirac, J. I. Criticality, the Area Law, and the Computational Power of Projected Entangled Pair States. *Phys. Rev. Lett.* **96**, 220601 (2006).

[24] Aharonov, D. & Ta-Shma, A. Adiabatic quantum state generation and statistical zero knowledge. In *STOC '03: Proceedings of the Thirty-Fifth Annual ACM Symposium on Theory of Computing*, 20–29 (ACM Press, New York, NY, 2003).

[25] Henley, C. L. From classical to quantum dynamics at Rokhsar–Kivelson Points. *J. Phys. Condens. Matter* **16**, S891–S898 (2004).

[26] Castelnovo, C., Chamon, C., Mudry, C. & Pujol, P. From quantum mechanics to classical statistical physics: Generalized Rokhsar–Kivelson Hamiltonians and the “Stochastic Matrix Form” decomposition. *Ann. Phys. (N. Y.)* **318**, 316–344 (2005).

[27] Seneta, E. *Non-negative Matrices and Markov Chains* (Springer, New York, NY, 1981).

[28] Aldous, D. J. Some Inequalities for Reversible Markov Chains. *J. London Math. Soc.* **s2-25**, 564–576 (1982).

[29] Glauber, R. J. Time-Dependent Statistics of the Ising Model. *J. Math. Phys.* **4**, 294–307 (1963).

[30] Felderhof, B. Spin relaxation of the Ising chain. *Rep. Math. Phys.* **1**, 215–234 (1971).

[31] Siggia, E. D. Pseudospin formulation of kinetic Ising models. *Phys. Rev. B* **16**, 2319–2320 (1977).

[32] Rokhsar, D. S. & Kivelson, S. A. Superconductivity and the Quantum Hard-Core Dimer Gas. *Phys. Rev. Lett.* **61**, 2376–2379 (1988).

[33] Bravyi, S. & Terhal, B. Complexity of Stoquastic Frustration-Free Hamiltonians. *SIAM J. Comput.* **39**, 1462–1485 (2010).

[34] Skrovseth, S. O. & Bartlett, S. D. Phase transitions and localizable entanglement in cluster-state spin chains with Ising couplings and local fields. *Phys. Rev. A* **80**, 022316 (2009).

[35] Niu, Y. *et al.* Majorana zero modes in a quantum Ising

chain with longer-ranged interactions. *Phys. Rev. B* **85**, 035110 (2012).

[36] Son, W., Amico, L. & Vedral, V. Topological order in 1D Cluster state protected by symmetry. *Quantum Inf. Process.* **11**, 1961–1968 (2011).

[37] Levin, D. A., Peres, Y. & Wilmer, E. L. *Markov Chains and Mixing Times* (American Mathematical Society, Providence, RI, 2009).

[38] Nielsen, M. A. & Chuang, I. L. *Quantum Computation and Quantum Information* (Cambridge University Press, Cambridge, 2010).

[39] Dyer, M., Sinclair, A., Vigoda, E. & Weitz, D. Mixing in time and space for lattice spin systems: A combinatorial view. *Random Struct. Algor.* **24**, 461–479 (2004).

[40] Sly, A. Computational Transition at the Uniqueness Threshold. In *51st Annual Symposium on Foundations of Computer Science*, 287–296 (IEEE Computer Society, Los Alamitos, CA, 2010).

[41] Gaunt, D. S. & Fisher, M. E. Hard-Sphere Lattice Gases. I. Plane-Square Lattice. *J. Chem. Phys.* **43**, 2840–2863 (1965).

[42] Weigt, M. & Hartmann, A. K. Minimal vertex covers on finite-connectivity random graphs: A hard-sphere lattice-gas picture. *Phys. Rev. E* **63**, 056127 (2001).

[43] Hastings, W. K. Monte Carlo sampling methods using Markov chains and their applications. *Biometrika* **57**, 97–109 (1970).

[44] Fendley, P., Sengupta, K. & Sachdev, S. Competing density-wave orders in a one-dimensional hard-boson model. *Phys. Rev. B* **69**, 075106 (2004).

[45] Lesanovsky, I. Liquid Ground State, Gap, and Excited States of a Strongly Correlated Spin Chain. *Phys. Rev. Lett.* **108**, 105301 (2012).

[46] Bernien, H. *et al.* Probing many-body dynamics on a 51-atom quantum simulator. *Nature* **551**, 579–584 (2017).

[47] Lloyd, S. Universal Quantum Simulators. *Science* **273**, 1073–1078 (1996).

[48] Glaetzle, A. W. *et al.* Quantum Spin-Ice and Dimer Models with Rydberg Atoms. *Phys. Rev. X* **4**, 041037 (2014).

[49] Pichler, H., Wang, S.-T., Zhou, L., Choi, S. & Lukin, M. D. Quantum Optimization for Maximum Independent Set Using Rydberg Atom Arrays. Preprint at <http://arxiv.org/abs/1808.10816> (2018).

[50] Wu, J. & Hsieh, T. H. Variational Thermal Quantum Simulation via Thermofield Double States. *Phys. Rev. Lett.* **123**, 220502 (2019).

## ACKNOWLEDGMENTS

The authors thank J. I. Cirac, E. A. Demler, A. Polkovnikov, and P. Zoller for insightful discussions. We acknowledge support from the National Science Foundation, the MIT–Harvard Center for Ultracold Atoms, the Department of Energy, and the DARPA ONISQ program. DS acknowledges support from the FWO as post-doctoral fellow of the Research Foundation – Flanders. HP acknowledges support by the Gordon and Betty Moore Foundation.

## METHODS

### Adiabatic sweeps

The rate of change of the Hamiltonian parameters are chosen to satisfy the adiabatic condition at every point along a given path [51, 52]. For a general set of parameters  $\lambda_\mu$ , we let

$$\sum_{\mu, \nu} g_{\mu\nu} \frac{d\lambda_\mu}{dt} \frac{d\lambda_\nu}{dt} = \varepsilon^2, \quad (5)$$

where  $\varepsilon$  is a small, dimensionless number and

$$g_{\mu\nu} = \sum_{k \neq 0} \frac{\langle \partial_\mu 0 | k \rangle \langle k | \partial_\nu 0 \rangle}{(E_k - E_0)^2}. \quad (6)$$

Here the  $|k\rangle$  and  $E_k$  label the eigenstates and corresponding eigenenergies of the system with  $k = 0$  denoting the ground state. The notation  $\partial_\mu$  is a shorthand for  $d/d\lambda_\mu$ . Equations (5) and (6) ensure that the parameters change slowly when the gap is small while simultaneously taking into account the matrix elements  $\langle k | \partial_\mu 0 \rangle$ , which determine the coupling strength of nonadiabatic processes to a particular excited state  $|k\rangle$ . The total evolution time can be adjusted by varying  $\varepsilon$  and is given by

$$t_{\text{tot}} = \frac{1}{\varepsilon} \int \sqrt{\sum_{\mu, \nu} d\lambda_\mu d\lambda_\nu g_{\mu\nu}}, \quad (7)$$

where the integral runs along the path of interest.

We show in the SI that for the cases studied here, a constant fidelity close to unity is reached at a small value of  $\varepsilon$  that is independent of  $n$ . Hence, the parametric dependence of the adiabatic state preparation time on  $n$  only depends on the integral in equation (7). Indeed, we find that the scalings along the various paths for the 1D Ising model can be analytically established from the singular properties of  $g_{\mu\nu}$  at the tricritical point. A similar numerical analysis is provided in the SI for both of the independent set problems.

### Implementation with Rydberg atoms

For unit disk graphs, the parent Hamiltonian for the weighted independent set problem, equation (4), can be efficiently implemented using highly excited Rydberg states of neutral atoms [49]. As illustrated in Fig. 3b, the ground state  $|g_i\rangle$  of an atom  $i$  encodes the unoccupied state of a given vertex  $i$ . Similarly, the occupied state is encoded in a Rydberg state  $|r_i\rangle$ . We implement the first and last term in equation (4) by driving a transition from  $|g_i\rangle$  to  $|r_i\rangle$ . The value of  $V_{e,i}$  is set by the detuning of the drive, whereas  $\Omega_i$  is proportional to the amplitude of the drive,  $\mathcal{E}_i$ . The projectors  $P_i$  arise due to Rydberg

blockade. If an atom is excited to the Rydberg state, the strong van der Waals interaction  $U_{\text{vdW}}$  shifts the Rydberg states of all neighboring atoms out of resonance, effectively turning off the drive and thereby enforcing the independent set constraint. The remaining second term in equation (4) can be realized using a similar approach, combining the Rydberg blockade with an AC Stark shift induced by an off-resonant drive from the ground state to an auxiliary Rydberg state  $|r'_i\rangle$ . The Rydberg interaction contributes additional terms to the Hamiltonian that decay as  $1/r^6$  with the distance  $r$  between two atoms. We have neglected these terms throughout, noting that a strategy to mitigate their role has been proposed in a related context [53].

Interactions between Rydberg atoms can also be used to implement more complicated parent Hamiltonians. For instance, Förster resonances between Rydberg states can give rise to simultaneous flips of two neighboring spins [54]. Such updates allow defects of two adjacent, unoccupied vertices to diffuse without an energy barrier. This results in a gap  $\Delta \sim 1/n^2$  at low temperature along the one-parameter family  $H_q(\beta)$  without the factor  $e^{-\beta}$ . Hence, the corresponding Markov chain samples quadratically faster from the ground state than the Markov chain with only single spin flips. The quantum algorithm does not experience a parametric speedup with these updates as the computation time is limited by the time for correlations to spread over the entire system. Both the classical and quantum algorithms associated with correlated updates will be discussed in detail elsewhere.

Finally, we note that even though the star graph is not a unit disk graph, its parent Hamiltonian could potentially be implemented using anisotropic interactions between Rydberg states [48].

### Classical phase transition of the star graph

The temperature at which the classical model associated with the weighted independent set problem for the star graph undergoes a phase transition can be computed exactly. The partition function is given by

$$\mathcal{Z} = (1 + 2e^\beta)^b + e^{b\beta} (1 + e^\beta)^b. \quad (8)$$

The two terms correspond to the different configurations of the central vertex. The probability that the central site is occupied is given by

$$p_1 = \frac{1}{\mathcal{Z}} e^{b\beta} (1 + 2e^\beta)^b = \left[ 1 + \left( \frac{1 + 2e^\beta}{e^\beta + e^{2\beta}} \right)^b \right]^{-1}. \quad (9)$$

In the thermodynamic limit  $b \rightarrow \infty$ , this turns into the step function  $p_1 = \Theta(\beta - \beta_c)$ , where  $\beta_c = \log \varphi$  with  $\varphi = (\sqrt{5} + 1)/2$  being the golden ratio. The entropy  $S = \beta(U - F)$  can be computed from the Helmholtz

free energy  $F = -\log \mathcal{Z}/\beta$  and the total energy  $U = -\partial \log \mathcal{Z}/\partial \beta$ .

## Two-state model for the star graph

The star graph has three types of vertices: the vertex at the center and the inner and outer vertices on each branch. Restricting our analysis to the subspace that is completely symmetric under permutations of the branches, we introduce the total occupation numbers  $n_{\text{in}} = \sum_{i=1}^b n_{\text{in},i}$  and  $n_{\text{out}} = \sum_{i=1}^b n_{\text{out},i}$  as well as the number of unoccupied branches  $n_0$ . The symmetric subspace is spanned by the states  $|n_{\text{cen}}, n_{\text{in}}, n_{\text{out}}, n_0\rangle$ , where  $n_{\text{cen}} \in \{0, 1\}$ , while the other occupation numbers are nonnegative integers satisfying  $n_{\text{in}} + n_{\text{out}} + n_0 = b$ . If  $n_{\text{cen}} = 1$ , the independent set constraint further requires  $n_{\text{in}} = 0$ . The state  $|n_{\text{cen}}, n_{\text{in}}, n_{\text{out}}, n_0\rangle$  is an equal superposition of  $b!/(n_{\text{in}}! n_{\text{out}}! n_0!)$  independent configurations.

The permutation symmetry leads to a bosonic algebra. We define the bosonic annihilation operators  $b_{\text{in}}$ ,  $b_{\text{out}}$ , and  $b_0$  respectively associated with the occupation numbers  $n_{\text{in}}$ ,  $n_{\text{out}}$ , and  $n_0$ . The Hamiltonian can be split into blocks where the central vertex is either occupied or unoccupied as well as an off-diagonal term coupling them. Explicitly,

$$H_q = H_q^{(0)} \otimes (1 - n_{\text{cen}}) + H_q^{(1)} \otimes n_{\text{cen}} + H_q^{(\text{od})} \otimes \sigma_{\text{cen}}^x. \quad (10)$$

It follows from equation (4) that in terms of the bosonic operators

$$\begin{aligned} H_q^{(0)} = & V_{e,\text{in}} b_{\text{in}}^\dagger b_{\text{in}} + V_{e,\text{out}} b_{\text{out}}^\dagger b_{\text{out}} + (V_{g,\text{in}} + V_{g,\text{out}}) b_0^\dagger b_0 \\ & - \Omega_{\text{in}} (b_{\text{in}}^\dagger b_0 + \text{h.c.}) - \Omega_{\text{out}} (b_{\text{out}}^\dagger b_0 + \text{h.c.}) \\ & + V_{g,\text{cen}} P(n_{\text{in}} = 0), \end{aligned} \quad (11)$$

$$\begin{aligned} H_q^{(1)} = & V_{e,\text{out}} b_{\text{out}}^\dagger b_{\text{out}} + V_{g,\text{out}} b_0^\dagger b_0 \\ & - \Omega_{\text{out}} (b_{\text{out}}^\dagger b_0 + \text{h.c.}) + V_{e,\text{cen}}, \end{aligned} \quad (12)$$

$$H_q^{(\text{od})} = -\Omega_{\text{cen}} P(n_{\text{in}} = 0), \quad (13)$$

where  $P(n_{\text{in}} = 0)$  projects onto states with no occupied inner vertices. The parameters are labeled in accordance to the definitions in equation (4) with the vertex index  $i$  replaced by the type of the vertex.

To diagonalize the Hamiltonian, we treat  $P(n_{\text{in}} = 0)$  perturbatively. We identify the lowest energy modes that diagonalize the quadratic parts of  $H_q^{(0)}$  and  $H_q^{(1)}$  and associate with them the bosonic annihilation operators  $c_0$  and  $c_1$ , respectively. Both modes have zero energy while the other modes are gapped for any finite value of  $\beta$ . We may thus expect the ground state to be well approximated in the subspace spanned by  $|\psi_0\rangle = c_0^{\dagger b} |0\rangle / \sqrt{b!}$  and  $|\psi_1\rangle = c_1^{\dagger b} |0\rangle / \sqrt{b!}$ , where  $|0\rangle$  denotes the bosonic vacuum. We focus on the situation where all parameters follow the one-parameter family  $H_q(\beta)$  except for  $\Omega_{\text{cen}}$  and  $V_{e,\text{cen}}$ , which may be adjusted freely. One can show that in this

case,  $|\psi_0\rangle$  and  $|\psi_1\rangle$  correspond to the Gibbs state of the star with the central vertex held fixed.

To include the effect of the terms involving  $P(n_{\text{in}} = 0)$ , we perform a Schrieffer–Wolff transformation for the subspace spanned by  $|\psi_0\rangle$  and  $|\psi_1\rangle$  [55]. We arrive at the effective Hamiltonian

$$H_{\text{eff}} = \begin{pmatrix} \varepsilon_0 + \delta\varepsilon_0 & -J - \delta J \\ -J - \delta J & V_{e,\text{cen}} + \delta\varepsilon_1 \end{pmatrix}, \quad (14)$$

where the terms

$$\varepsilon_0 = \langle \psi_0 | P(n_{\text{in}} = 0) | \psi_0 \rangle = \left( \frac{1 + e^\beta}{1 + 2e^\beta} \right)^b, \quad (15)$$

$$J = \Omega_{\text{cen}} \langle \psi_1 | P(n_{\text{in}} = 0) | \psi_0 \rangle = \Omega_{\text{cen}} \left( \frac{1 + e^\beta}{1 + 2e^\beta} \right)^{b/2} \quad (16)$$

are obtained by projecting the full Hamiltonian onto the low-energy subspace. The corrections from coupling to excited states as given by the Schrieffer–Wolff transformation up to second order are

$$\delta\varepsilon_0 = -\varepsilon_0 \sum_n \frac{1}{E_n^{(0)}} \left| \langle E_n^{(0)} | \sigma_{\text{cen}}^x | \psi_1 \rangle \right|^2, \quad (17)$$

$$\delta\varepsilon_1 = -\Omega_{\text{cen}}^2 \sum_n \frac{\left| \langle E_n^{(0)} | \sigma_{\text{cen}}^x | \psi_1 \rangle \right|^2}{E_n^{(0)} - V_{e,\text{cen}}}, \quad (18)$$

$$\begin{aligned} \delta J = & -\frac{1}{2} \Omega_{\text{cen}} \sqrt{\varepsilon_0} \sum_n \left( \frac{1}{E_n^{(0)}} + \frac{1}{E_n^{(0)} - V_{e,\text{cen}}} \right) \\ & \times \left| \langle E_n^{(0)} | \sigma_{\text{cen}}^x | \psi_1 \rangle \right|^2. \end{aligned} \quad (19)$$

Here, we made use of the relation  $P(n_{\text{in}} = 0) | \psi_0 \rangle = \sqrt{\varepsilon_0} \sigma_{\text{cen}}^x | \psi_1 \rangle$ , which holds along the paths of interest. The sums run over all excited states  $|E_n^{(0)}\rangle$  with energy  $E_n^{(0)}$  of the quadratic part of  $H_q^{(0)}$  (excluding  $|\psi_0\rangle$ ). We will neglect the term  $V_{e,\text{cen}}$  in the energy denominators of equations (18) and (19), which is justified when  $V_{e,\text{cen}}$  is small compared to  $E_n^{(0)}$ . The discussion remains valid even if this is not the case because the second-order corrections from the Schrieffer–Wolff transformation can then be ignored. Combining these results, the complete effective Hamiltonian may be written as

$$H_{\text{eff}} = \begin{pmatrix} (1-f)\varepsilon_0 & -(1-f)J \\ -(1-f)J & V_{e,\text{cen}} - f\Omega_{\text{cen}}^2 \end{pmatrix}, \quad (20)$$

where  $f = \sum_n \left| \langle E_n^{(0)} | \sigma_{\text{cen}}^x | \psi_1 \rangle \right|^2 / E_n^{(0)}$ . We find numerically that  $f$  decays as an inverse power law in  $b$  such that our approximations are well justified in the thermodynamic limit (see SI). Along the one-parameter family  $H_q(\beta)$ , we have  $V_{e,\text{cen}} = \Omega_{\text{cen}}^2$ . Hence,  $H_{\text{eff}}$  depends on  $f$  only through an overall factor  $(1-f)$ , which tends to 1 in the limit of large  $b$ . The phase transition of the underlying classical model manifests itself as a first-order

quantum phase transition from  $|\psi_0\rangle$  to  $|\psi_1\rangle$ . The transition occurs when the two states are resonant,  $\varepsilon_0 = V_{e,\text{cen}}$ , which can be solved to give  $\beta_c = \log \varphi$  as expected.

---

[51] Messiah, A. *Quantum Mechanics* (Dover Publications, Mineola, NY, 2014).  
 [52] Rezakhani, A. T., Kuo, W.-J., Hamma, A., Lidar, D. A.

& Zanardi, P. Quantum Adiabatic Brachistochrone. *Phys. Rev. Lett.* **103**, 080502 (2009).  
 [53] Pichler, H., Wang, S.-T., Zhou, L., Choi, S. & Lukin, M. D. Computational complexity of the Rydberg blockade in two dimensions. Preprint at <http://arxiv.org/abs/1809.04954> (2018).  
 [54] Barredo, D. *et al.* Coherent Excitation Transfer in a Spin Chain of Three Rydberg Atoms. *Phys. Rev. Lett.* **114**, 113002 (2015).  
 [55] Bravyi, S., DiVincenzo, D. P. & Loss, D. Schrieffer–Wolff transformation for quantum many-body systems. *Ann. Phys. (N. Y.)* **326**, 2793–2826 (2011).